Rhinology Online

ORIGINAL CONTRIBUTION

OPEN ACCESS

Advanced CT imaging demonstrating the bulla lamella and the basal lamella of the middle turbinate as endoscopic landmarks for the anterior ethmoid artery*

S. J. Zinreich[1], H. Stammberger[2], W. Bolger[3], M. Solaiyappan[1], M. Ishii[4]

[1] The Russel H. Morgan Department of Radiology, The Johns Hopkins Medical Institutions, Baltimore, MD, USA

[2] Department of General Otorhinolaryngology-Head and Neck Surgery, Medical University Graz, Austria

[3] North Florida Sinus Center, Jacksonville, FL, USA

[4] The Department of Otorhinolaryngology Head and Neck Surgery, The Johns Hopkins Medical Institutions, Baltimore, MD, USA

Rhinology Online, Vol 2: 32 - 43, 2019

http://doi.org/10.4193/RHINOL/18.082

***Received for publication:**

November 27, 2018

Accepted: February 12, 2019

Published: March 7, 2019

Abstract

Objective: Our objective is to show how the use of Computer Tomography (CT) multiplanar displays (MPR) and 3D Stereoscopic Imaging (3DSI), can provide precise anatomical landmarks to identify the location of the Anterior Ethmoid Artery (AEA) during endoscopic sinus surgery (FESS).

Materials and Methods: The study comprised 48 patients, representing 96 nasal cavity/sinus sides. The anterior ethmoid foramen was the landmark that defined the entry of the AEA into the ethmoid on CT MPR and 3DSI, and anatomic relationships closely related to to the AEA were recorded.

Results: The anterior ethmoidal foramen (AEF) was associated with the bulla lamella (BL) in 46.9% of cases, and the basal lamella of the middle turbinate (BLMT) in 31.6%. In 7.1% of cases, the AEF was associated with both lamellae. Similarly, at the AES, the AEF was associated with the BL and BLMT in 72.5% and 46.9% of cases, respectively. In 29.6%, the AEA was associated with both lamellae. In 48%, the AEF and AES were at or in the bone of the ethmoidal roof/ skull base. In 48%, the AEA, the AEF, and the AES were in the same coronal plane, indicating a straight horizontal course across the ethmoid. In the remaining samples, the AES was anterior to the AEF, indicating an oblique course of the AEA.

Conclusion: This study demonstrates that 3DSI imaging provides improved localization of the AEA, and establishes recognizable anatomic landmarks for endoscopically guided surgery, thus, preventing inadvertent complications.

Key words: anterior ethmoidal artery, bulla lamella, basal lamella of middle turbinate, anterior ethmoid sinus artery landmarks, 3D stereoscopic imaging of sinuses, CT multiplanar reconstruction of sinuses

Introduction

Functional Endoscopic Sinus Surgery (FESS) has been practiced worldwide for the past four decades following the principles initially established by Messerklinger, Stammberger, Kennedy and others [1-3]. Major complications – albeit relatively rare (between 0.4 – 1.5 percent), include lesions to the optic nerve, internal carotid artery, skull base , and dura, as well as intracranial and intra-orbital injury [4-6]. Surgical injury of the anterior ethmoidal artery (AEA) at or close to the lamina papyracea, "carries the risk of the proximal stump of the artery to retract into the orbit whilst continuing to hemorrhage, potentially leading to the serious consequence of visual loss" [6]. Preoperative evaluation of the imaging information accurately and reliably identifies the location of the AEA and provides safe surgical guidance, thus avoiding inadvertent lesions and their potential dramatic sequelae.

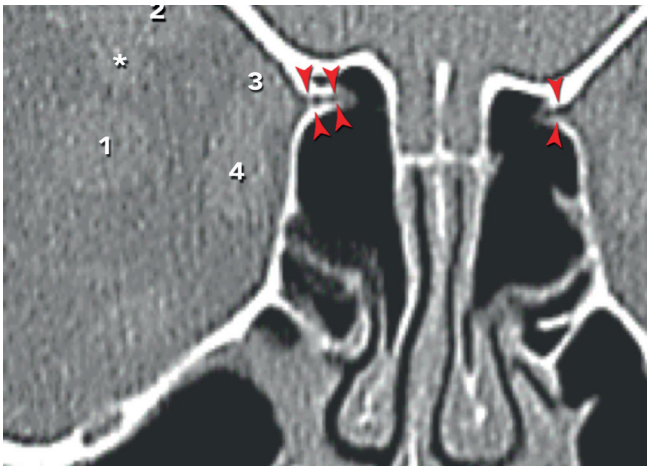

Figure 1. CT coronal plane demonstrating the site of the AEA foramen: arrowheads outline the "funnel-shaped" AEA foramen; asterisk = orbital artery; 1= optic nerve; 2 = superior orbital muscle; 3 = superior oblique muscle; 4 = medial rectus muscle.

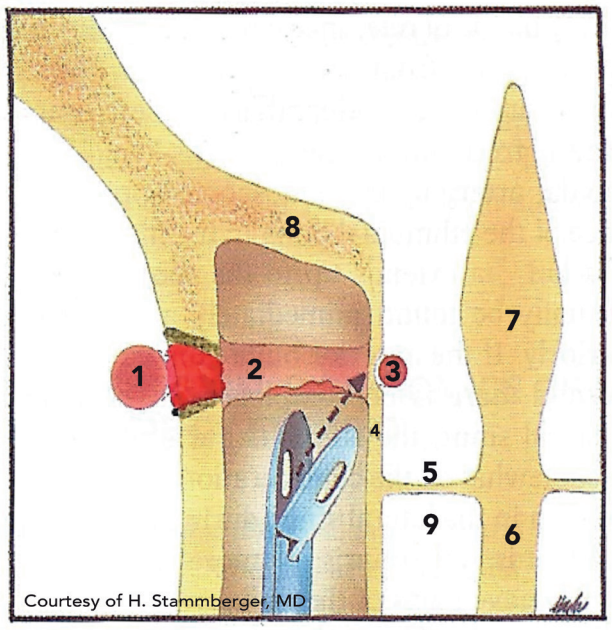

Figure 2. Surgical instrument approaching a dehiscent AEA canal within the ethmoidal sulcus: 1= site of intra-orbital anterior ethmoid foramen opening; 2 – AEA in bony canal traversing the ethmoid; 3 = AEA after penetration of lateral lamella of the cribriform plate in the "ethmoidal sulcus"; 4 = lateral lamella of the cribriform plate; 5 = cribriform plate; 6 = nasal septum; 7 = crista galli; 8 = frontal bone; 9 = olfactory fossa.

Since its introduction in the mid-1980s, CT imaging technology has advanced significantly allowing improved diagnosis and improved demonstration of the varied individual sino-nasal anatomy [7]. These advances have enabled surgeons to better prepare for surgery and avoid complications. Nevertheless, a persistent difficulty prevails in correlating the imaging information with the endoscopically viewed surgical field, which, in turn, may be an underlying factor in continued surgical complications, such as orbital injury and CSF leak [4-6].

The accurate identification of the AEA is cited on CT as a key anatomic landmark in preventing orbital and intracranial complications [2,3,8]. A precise understanding of the AEA location, its anatomic variations, and its relationship to the adjacent anatomy, is, therefore, important. However, the information currently provided by Computer X Ray Tomography Multiplanar Reconstructed Images CTMPR images appears visually different than the images presented to the surgeon via the endoscope. This explains the difficulty in establishing specific and recognizable anatomic landmarks that could be followed during surgery to avoid AEA-related complications.

The objective of this study was to show how to employ the currently available CTMPR, and the newly created 3DSI technology, in both a static and dynamic mode, and identify anatomic landmarks, which, in turn, locate the AEA, improve the correlation of the information provided by CT and endoscopy, and enhance pre-operative planning and intra-operative performance of FESS.

The bulla lamella (BL), the basal lamella of the middle turbinate (BLMT), and the base of skull (BS) serve as fundamental landmarks for FESS and are known to be in close proximity to the AEA and its course through the ethmoid. To date, using the available standard CT information, the relationship of the AEA to surgically well identifiable structures—the skull base, the bulla lamella, and the middle turbinate basal lamella—has not been established.

Our aim is to define the relationship between these four structures based on the information provided by new imaging technologies, and show how these landmarks can guide a safe surgical procedure.

Singer credits Eustachius (1520-1574) with the introduction of the study of human anatomical variability; however, it has been clear since Galen's time that humans are not homogeneous with respect to their anatomic construction [9]. Rather, people sometimes cluster into distinct anatomic subtypes. It is our central hypothesis that this is also the case for the anterior ethmoid artery. We, therefore, used a Gaussian mixture model approach to formally elucidate the distinct subtypes of AEA morphology and the variability within and between these subtypes. To the best of our knowledge, this is the first example of a Gaussian mixture model approach to illustrate clustering of anterior ethmoid and skull base anatomy into distinct anatomic subtypes.

Anatomy of the AEA

The AEA originates from the ophthalmic artery. It then courses between the superior oblique and medial rectus muscles to reach the anterior ethmoidal foramen, which opens into the lamina papyracea. This "opening" is pyramidal or funnel-shaped,

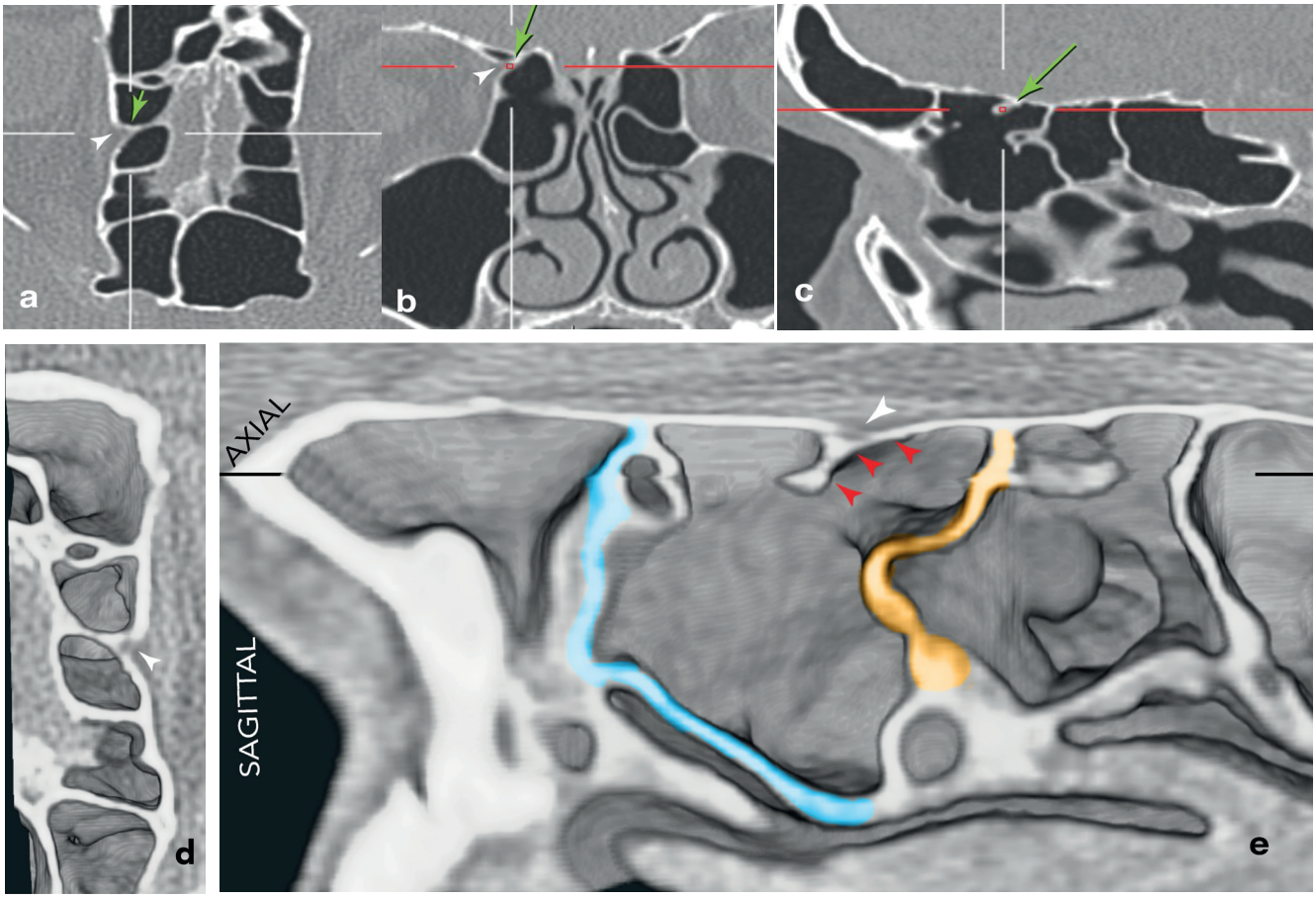

Figure 3. The AEA is in between the bulla lamella and the basal lamella. (a-c) CTMPR images, with the green arrow pointing to the center of the "cross-hairs," the focal point, shared by the three orthogonal planes, along the lateral course of the artery. The white arrowhead points to the origin of the AEA foramen. 3DSI images: (d) 3D volume viewing the axial plane from above, shows the origin of the AEA foramen as it "breaks" the lamina papyracea, and the course of the AEA is outlined with red arrowheads; (e) the 3D volume shows the somewhat oblique axial plane with the course of the AEA (red arrowheads). The lateral nasal wall is shown in the sagittal perspective, revealing the relationship with the basal lamella (mustard color), and the bulla lamella (blue).

and is well recognized on a CT coronal plane scan (Figure 1), as well as on an artist's representation (Figure 2), and on 3DSI image in the axial plane (Figures 3d,4f,5d,6d).

The AEA subsequently crosses the anterior ethmoid complex in a variable bony canal (anterior ethmoidal canal) to penetrate the lateral lamella of the cribriform plate into the olfactory fossa. Here, the AEA turns anteriorly and for 3 – 16 mm runs in a shallow groove of the lateral lamella, the so-called ethmoidal sulcus, the site of origin of the anterior meningeal artery. The AEA then reaches the nasal cavity through the cribriform-ethmoidal foramen and the lamina cribrosa. In the nasal cavity, it divides into the anterior nasal artery and various smaller branches. During its course along the ethmoidal sulcus, the AEA can be found intra -as well as- extradural, with the bony sulcus thinning the lateral lamella of the cribriform plate to 0.2mm. Thus, this area is the thinnest and least resistant bone within the anterior skull base [2,10] (Figure 2).

Methods

Imaging data

Axial CT scans were performed on a Siemens CT scanner using 0.7 mm thick slices, which yielded a volumetric image of the maxillo-facial structures. Studies were performed without administration of intravenous contrast material. The Multiplanar Reconstruction (MPR) programs were performed with Carestream Vue and Siemens Sygo.via software programs, which provide a simultaneous display of axial, coronal, and sagittal planes (Figures 3-6 a-c and Figure 4 d,e). Simultaneous display of the intranasal/sinus anatomy, relevant to the surgeon's planning and execution of the FESS procedure, were available. Our study primarily focused on the anatomy relevant for the identification of the AEA foramen and the intra nasal and or intracranial segment of the AEA. When necessary the Siemens Syngo.via software program was used to provide non-orthogonal plane reconstructions, as well as a dynamic displays of challenging

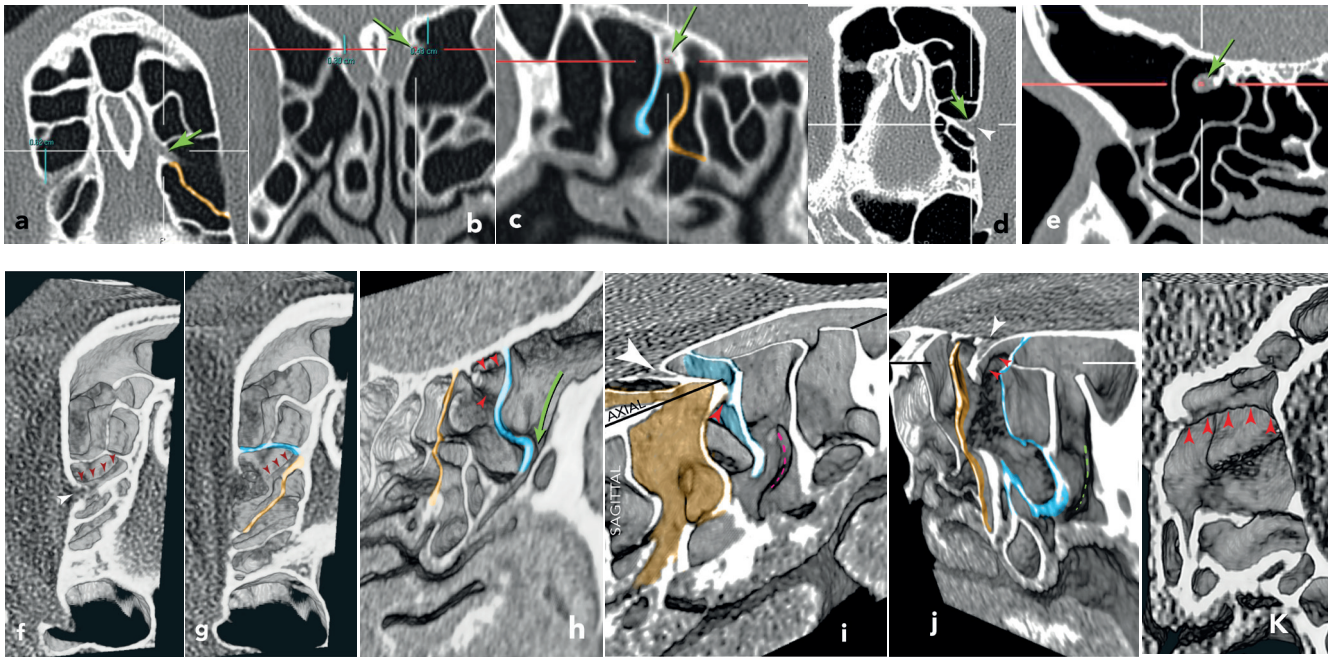

Figure 4. The AEA merging with the bulla lamella and the basal lamella. (a-c) CTMPR images, with the green arrow pointing to the center of the "cross-hairs," the focal point, shared by the three orthogonal planes, along the medial course of the artery, and images (d,e) with the "cross-hairs" centered along the lateral course of the AEA within the ethmoid sinus. The white arrowhead points to the origin of the AEA foramen, in image (d). The mustard color outlines the basal lamella, and the blue color the bulla lamella. 3DSI images (f-k) reveal the course of the AEA (red arrowheads) from laterally to medially. Green arrow (h), represents the opening of the frontal recess. Dashed red and green curved lines represent the hiatus semilunaris (i and j). The course of the artery is best demonstrated from lateral to medial on the 3D image presented from the coronal point of view (k). The bulla lamella is outlined in blue and the basal lamella is outlined in the mustard color. Note that medially (j), the artery adheres to both the bulla lamella and the basal lamella.

anatomic detail.

To establish and confirm the relationship of the AEA with the frontal recess, the uncinate process, the ethmoid bulla, the bulla lamella, and the supra-bullar recess spaces, a 3DSI display of the CT data (an advanced evolution of the Dextroscope imaging device) was used to validate and clearly show specific anatomic landmarks that would identify the location of the AEA, given the correlation between the 3DSI and the endoscopic view of the surgical site (Figures 3,5,6 d,e, and Figure 4, f-j).

An essential, key feature of our software is that it provides a 3D stereoscopic representation of the anatomy when viewed using a pair of electronic glasses. This enables the viewer to appreciate the depth of a structure, just as it would naturally be perceived, in the "real-world." Our challenge is to create the same effect as we display the 3D stereoscopic formatted structure onto a "flat" surface, without the necessity for electronic glasses, in a reasonably practical or economic manner. Therefore, here, the results are presented as volume-rendered images displayed on a flat surface, without the stereoscopic, depth-perception effect, and therefore, the images are a "simulated" 3D display.

Source of imaging data

The evaluated imaging data was of patients who had virtually no inflammatory disease within the nasal cavity and paranasal sinuses, and were selected by SJZ from his routine list of cases he was assigned to evaluate. Forty-eight patients (96 sides) were included in this study. A retrospective study was performed on de-identified CT data in accordance with the Johns Hopkins IRB regulations.

Evaluation methods

Computed X-ray Tomography with Multiplanar Reconstruction Evaluation (CTMPR)

1. MPR (axial, coronal, and sagittal) images were simultaneously displayed.
2. The AEA foramen was identified as it "broke" the continuity of the lamina papyracea, on the axial and/or the coronal plane (Figsure 3-6a, 3b,4d)
3. The crosshair that correlated the specific anatomic point on the axial, and /or coronal and sagittal image was placed on the AEA foramen medial to the "break" into the lamina papyracea, and the specific anatomic point was spontaneously displayed on all MPR images (axial, coronal, and

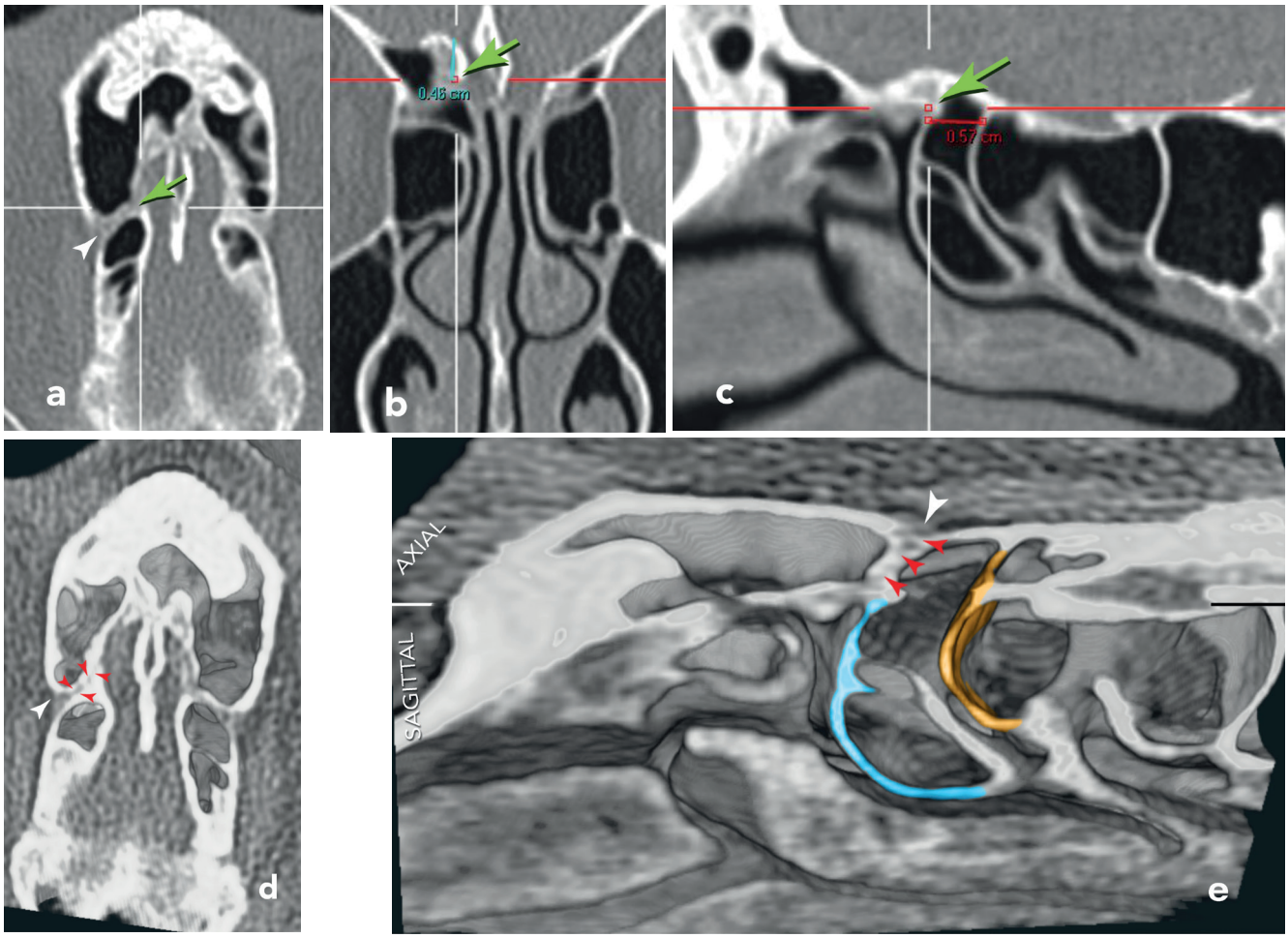

Figure 5. AEA coursing along the bulla lamella. a-c) CTMPR images in the axial, coronal, and sagittal planes with green arrow pointing to the site of "cross-registration" of the orthogonal planes, along the medial course of the artery. White arrow represents the site of origin of the AEA foramen. 3DSI images: (d) 3D volume viewing the axial plane from above, shows the origin of the AEA foramen as it "breaks" the lamina papyracea, and the course of the AEA is outlined by red arrows; (e) the 3D volume shows the somewhat oblique axial plane in the course of the AEA (red arrowheads), and the lateral nasal wall in the sagittal perspective, which revealed the relationship with the bulla lamella (blue), and the basal lamella (mustard color).

sagittal) (Figures 3a-c, and 4d,e).

4. Similarly, a separate evaluation was performed with the crosshairs placed at the medial point of the AEA within the skull base or within the anterior ethmoid. This medial "point" was established on the axial and coronal images, with the sagittal plane at the most medial portion of the anterior ethmoidal artery canal within the ethmoidal complex (Figures 4-6a-c). The following distances were recorded: AEA to bulla lamella; AEA to basal lamella; and bulla lamella to basal lamella (Table 1).
5. The axial plane was used to evaluate the angulation of the course of the AEA within the ethmoid sinus. When the AEA was in the skull base, the angulation within the skull base covering the ethmoid sinus was recorded, identifying the least and most angled course of the artery (Figures 3a, 4d, 5a, 6a).
6. With the sagittal plane(s) just medial to the lamina papyracea at the penetration of the AEA through the foramen, as well as at the level of the AES the following distances were recorded: AEA to bulla lamella; AEA to basal lamella; and bulla lamella to basal lamella (Table 1).

3D stereoscopic imaging evaluation

1. Stereoscopic 3D images (3DSI), were subsequently used to provide an "en block" 3D evaluation of this regional morphology.
2. The 3D imaged volume was "trimmed" medial to the nasal septum to evaluate the right and left sides separately. Thus, the "en block volume" was then positioned with the nose pointing anteriorly, the axial plane superiorly, and the lateral nasal wall anatomy revealed in the sagittal plane exposed medially. The imaging data in the axial plane was sequentially removed (in a scrolling manner) from superiorly to inferiorly until the AEA foramen within the lamina

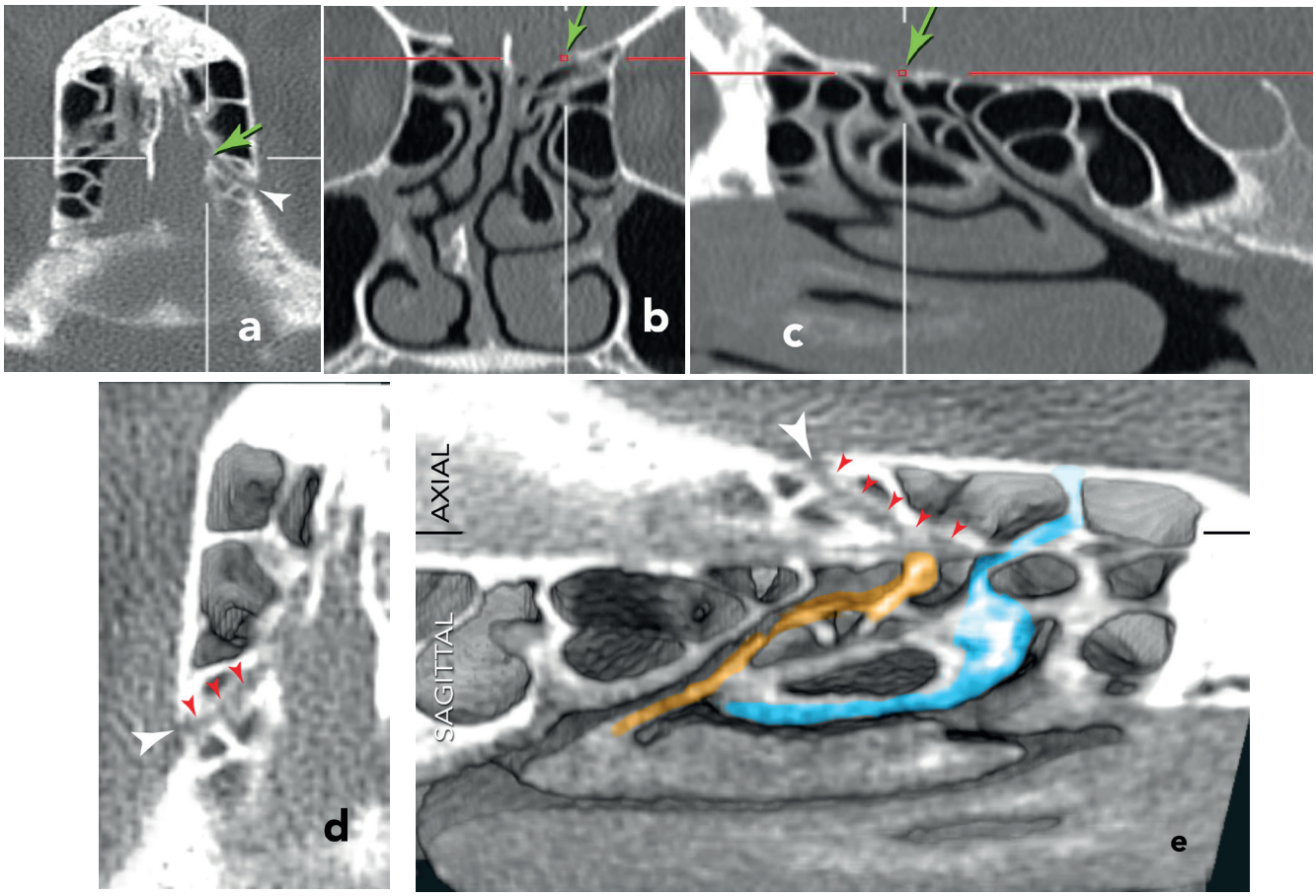

Figure 6. AEA coursing along the basal lamella. (a-c) CTMPR images, with the green arrow pointing to the center of the "cross-hairs," the focal point shared by the three orthogonal planes, along the medial course of the artery. The white arrowhead points to the origin of the AEA foramen.3DSI images: (d) 3D volume viewing the axial plane from above, shows the origin of the AEA foramen as it "breaks" the lamina papyracea, and the course of the AEA is outlined with red arrowheads; (e) the 3D volume shows the somewhat oblique axial plane in the course of the AEA (red arrowheads). The lateral nasal wall is shown in the sagittal perspective, which revealed the relationship with the basal lamella (mustard color), and the bulla lamella (blue).

papyracea was revealed (Figures 3, 5, 6 d, and 4f).

3. With the AEA foramen revealed on the axial image, the 3D volume was angled to expose the structures of the lateral nasal wall from the sagittal viewpoint. The 3D volume continued to be slightly angled in the medial direction (toward the evaluator), to maintain a view of the AEA foramen, but with greater focus on the anatomic structures to be best displayed within the lateral nasal wall (Figures 3, 5, 6e, and 4h,j).
4. A dynamic "scrolling," from medially to laterally, into the sagittal anatomy revealed the structures of the anterior ethmoid, and details about the morphology of the ethmoidal bulla, the bulla lamella, the uncinate process, the frontal recess, the supra orbital recess space(s), and the interconnectivity of the anterior osteo-meatal channels (OMC) (Figures 3, 5, 6e, and 4h-j).
5. Attention was directed to determine the specific relationships identified on the CTMPR evaluation, as detailed above, to corroborate and clarify, as well as add to the previously observed results obtained from the medial- and lateral-positioned sagittal orthogonal planes on the CTMPR evaluation. This also provided a 3D display of the structures directly related to the AEA, thus establishing the landmarks associated with the AEA.

Data analysis

We analyzed our data using Stata 15 (Stata Corp LLC, College Station, TX, USA). Our data had a bimodal distribution, so we used a finite mixture model regression with two classes to fit our data. We used a multinomial logistic distribution to estimate the probabilities for the latent classes. We estimated the posterior probability of class membership for all the data and assigned class membership based on the optimal decision rule. To deal with discretization of measurements that occur when measuring distances on a pixilated graph, we added subpixel Gaussian white noise to the measurements. This aided with the convergence of our regressions.

Results

In Table 1, we list the average distances measured from the AEA to the bulla lamella (BL), the basal lamella of the middle turbinate (BLMT), and the base of the skull (BS). We present both lateral and medial measurements. Positive numbers indicate that the structures of interest were anterior to the AEA while negative numbers indicate that they were posterior to the artery. In the case of the base of the skull measurements, positive numbers signify that the skull base was superior to the artery. In the same table, we also list the average distance measured between the medial and lateral AEAs. For these measurements, we used the lateral AEA as a reference and positive numbers indicate that the medial AEA measurement point was anterior to the lateral point.

In Figure 7, we plot a sample histogram for the lateral measurements, i.e., those made along the lamina papyracea, the AEA to BL measurements, to illustrate the key feature of this data set. This histogram is not unimodal (Hartigan's dip test: D=0.059, p = 0.011); rather, it is bimodal with a narrow hump centered at zero and a second wider one centered somewhere between 0.5 and 1.0 cm. The large sharp peak concentrated at zero signified that a fair number of our measurements were zero or near-zero. This indicates that, in a large number of subjects, the BL and AEA were either touching or nearly touching at the anterior ethmoidal foramen. The remaining data is broadly distributed. For these subjects, the AEA was distinct and separate from the BL. All measurements revealed this bimodal behavior, suggesting there are two distinct varieties of human anatomy in this area - those in whom the AEA is associated spatially with the lamella and structures we were studying and those in whom the AEA is separate. We formalized these observations with a Gaussian mixture model approach.

We present the results of these regressions in Tables 2 and 3. The finite mixture model results were used to estimate the probability of being in one of the two classes (touching or separate), while the class response model provided the mean or mode distance and variance of the measurements for each class. From Table 3, we see that the average lateral AEA to BL measurement for the touching and separate groups were 0.004 cm (-0.008-0.001) cm, and 0.632 cm (0.540-0.725) cm, respectively, for example. The 95% confidence intervals are shown in parentheses. The spread, i.e., standard deviation, in the touching group was very low, at 0.001 cm. We found the separate group spread to be much larger, at 0.107 cm. The corresponding medial and lateral class response regression coefficients tended to mirror each other while the finite mixture model coefficients did not. This implies that the average distances measured between corresponding medial and lateral structures were similar, e.g., the medial and lateral AEA to BLMT coefficients were -0.819 cm and -0.873 cm, respectively. The consequence of the unmatched, finite, mixture model coefficients results in different class membership probabilities laterally to medially. We present this data next.

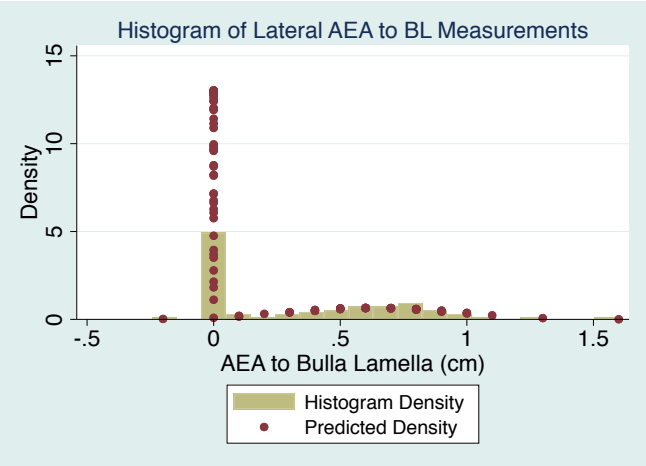

Figure 7. Histogram of the lateral anterior ethmoid artery (AEA) with regard to the bulla lamella (BL) measurements (bar graph), and the estimated density from a finite, mixture model regression (point plot).

We illustrate how class membership for different medial and lateral structures relate to each other with contingency Tables 4, 5, and 6. These tables show that, along the lamina papyracea, the AEA will be associated with at least one lamella 71.4% of the time, and that, 7.1% of the time, it will be associated with both lamella, i.e., the AEA, BL, and BLMT fuse into one complex. Similarly, with the medial measurements, we found that, in 89.8% of our cases, the AEA was associated with at least one lamella, and that, in 29.6% of the cases, it was associated with both lamella. These tables also demonstrate that the AEA is more likely to be associated with the BL than the BLMT. More specifically, the AEA abuts the BL 72.5% medially and 46.9% laterally; while it only touches the BLMT 46.9% medially and 31.6% laterally.

The BS contingency Table 5 tells a similar story. The chance that the AEA was embedded in the BS both medially and laterally was 40.8%. In 31.6% of cases, the AEA was separate from the BS on both sides; while, in the remaining 27.5% of cases, it was attached to the BS at one end, but not the other.

Table 6 illustrates how the probabilities that the AEA is associated with the BL and the BLMT both medially and laterally are quite different. For example, 35.7% of the time, the AEA was associated with the BL at one end, but not the other. This pattern holds for the BLMT, but with a slightly lower frequency of 27.5%. In general, we found that it was more likely for an AEA that was separate from a lamella laterally to join a lamella medially than vice versa.

In 48.0% of subjects, the medial and lateral AEA measurement points (anterior ethmoidal foramen and anterior ethmoidal sulcus) existed in the same coronal plane. In the remaining subjects, the artery ran in an oblique plane with the anterior ethmoidal sulcus displaced, on average, 0.3 cm anterior to the anterior ethmoidal foramen.

Table 1. Table to raw measurements.

Structure	Average Distance (cm)	Standard Deviation (cm)	95% Confidence Intervals for mean (cm)
Lateral			
Bulla Lamella	0.33	0.40	(0.26,0.42)
Basal Lamella	-0.61	0.57	-(0.72,0.49)
Base of Skull	0.18	0.20	(0.13,0.22)
Medial			
Bulla Lamella	0.19	0.36	(0.12,0.26)
Basal Lamella	-0.46	0.54	-(0.56,0.35)
Base of Skull	0.14	0.19	(0.11,0.18)
Medial to Lateral			
AEA to AEA	0.17	0.20	(0.13,0.21)

Table 2. Finite mixture model results for the lateral and medial bulla lamella, basal lamella, and base of skull regressions and the medial to lateral AEA regression.

	Finite mixture model		
	Coefficient	Standard error	95% Confidence Intervals
Lateral			
Bulla Lamella			
Class: Touching	Base		
Class: Separate	0.143	0.2075	(-0.263,0.550)
Basal Lamella MT			
Class: Touching	Base		
Class: Separate	0.828	0.227	(0.1272,0.384)
Base of Skull			
Class: Touching	Base		
Class: Separate	-0.117	0.203	(-0.515,0.281)
Medial			
Bulla Lamella			
Class: Touching	Base		
Class: Separate Constant	-0.961	0.226	-(-1.40,0.517)
Basal Lamella MT			
Class: Touching	Base		
Class: Separate Constant	0.130	0.203	(-0.268,0.528)
Base of Skull			
Class: Touching	Base		
Class: Separate Constant	-0.239	0.204	(-0.639,0.162)
Medial to Lateral			
AEA to AEA			
Class: Touching	Base		
Class: Separate Constant	0.097	0.204	(-0.303,0.497)

To illustrate how well our model fit the data, we superimposed the estimated density for our AEA to the BL model over the raw data histogram in Figure 7. For the wide mode, there was excellent agreement. It is important to appreciate that the area under the curve is the essential measure of comparison. The histogram bar at zero was much shorter than predicted because the base of the bar had a relatively wide fixed interval. The remaining data showed similar behaviors.

Discussion

In the early 1980s, Endoscopic Sinus Surgery (ESS), now referred to as Functional Endoscopic Surgery (FESS), replaced external approach procedures and is the treatment of choice for sinus and nasal pathologies, as well as skull base and orbital lesions [1-3]. The introduction of advanced endoscopes, surgical instruments, and imaging techniques, including image guidance, aided surgery procedures and improved the safety [1-3,7]. Over the past four decades, there has been a steady increase in the number of FESS procedures [4].

Unfortunately, given the close proximity of the surgical site to the orbit and the intracranial compartment, even though considerably reduced since the early days, the FESS procedure continued to be associated with a variety of complications, including inadvertent damage to the AEA, which resulted in intra-orbital and intracranial bleeding and epistaxis [4-6, 10-21].

Lund et al. reported that if the AEA is traumatized at the foramen of the artery (at the penetration through the lamina papyracea), this invariably results in retraction of the bleeding artery into the orbit, and that the injury is more frequent if the artery courses in the ethmoidal sinus below the skull base [6]. Hosemann and colleagues concurred and stated that the likelihood of damage to the artery increases the greater the distance from the skull base, and if in the basal lamella [4].

Since the introduction of FESS, surgeons have used CT imaging as a "road map" to guide the surgery in this complex and varied anatomic area [3,7,8]. Several authors have reported the use of coronal CT images, and subsequently, MPR images, and finally, Image -guided Surgery (IGS) based on MPRs of the CT information to site a variety of anatomic "landmarks" that were meant to determine the location of the AEA, and avoid inadvertent damage to this structure [10-13, 15-21]. The AEA foramen is still an established imaging landmark [12]. The "standard" coronal CT plane will accurately display the location of the AEA foramen, as demonstrated on the coronal images within the set of MPR displays provided with each of the cases in Figures 3-6. Howe-

Table 3. Class response model results for the lateral and medial bulla lamella, the basal lamella, and the base of the skull regressions and the medial to lateral AEA regression.

Class Response Model	Value (cm)	Standard Error (cm)	95% Confidence Intervals (cm)
Lateral			
Bulla Lamella			
Class: Touching Constant	-0.004	0.002	(-0.008,0.001)
Class: Touching Variance	0.001	<0.001	(0.0001,0.0003)
Class: Separate Constant	0.632	0.047	(0.540,0.725)
Class: Separate Variance	0.107	0.022	(0.072,0.160)
Basal Lamella MT			
Class: Touching Constant	-0.002	0.004	(-0.010,0.006)
Class: Touching Variance	0.0004	0.0001	(0.0003,0.0008)
Class: Separate Constant	-0.873	0.060	(-0.991,0.754)
Class: Separate Variance	0.235	0.041	(0.166,0.331)
Base of Skull			
Class: Touching Constant	-0.001	0.003	(-0.007,0.004)
Class: Touching Variance	0.0004	0.00008	(0.0003,0.0006)
Class: Separate Constant	0.370	0.016	(0.338,0.402)
Class: Separate Variance	0.012	0.003	(0.008,0.018)
Medial			
Bulla Lamella			
Class: Touching Constant	0.004	0.006	(-0.017,0.008)
Class: Touching Variance	0.0028	0.0005	(0.0019,0.0039)
Class: Separate Constant	0.698	0.074	(0.554,0.843)
Class: Separate Variance	0.107	0.037	(0.054,0.212)
Basal Lamella MT			
Class: Touching Constant	0.002	0.008	(-0.014,0.017)
Class: Touching Variance	0.002	0.0006	(0.001,0.004)
Class: Separate Constant	-0.819	0.070	(-0.957,0.681)
Class: Separate Variance	0.220	0.045	(0.147,0.329)
Base of Skull			
Class: Touching Constant	-0.0004	0.011	(-0.022,0.021)
Class: Touching Variance	0.004	0.001	(0.002,0.007)
Class: Separate Constant	0.324	0.047	(0.231,0.417)
Class: Separate Variance	0.028	0.010	(0.014,0.057)
Medial to Lateral			
AEA to AEA			
Class: Touching Constant	0.004	0.004	(-0.002,0.011)
Class: Touching Variance	0.0004	0.0001	(0.0003,0.0007)
Class: Separate Constant	0.300	0.026	(0.250,0.351)
Class: Separate Variance	0.028	0.006	(0.019,0.042)

Table 4. Contingency table for class membership, medial AEA to BL vs medial AEA to BLMT on the left and lateral AEA to BL vs lateral AEA to BLMT on the right.

Medial AEA to bulla lamella vs medial AEA to basal lamella of the middle turbinate			
	Basal Lamella of the Middle Turbinate		
Bulla Lamella	Separate from AEA	At AEA	Total
Separate from AEA	10 (10.2)%)	17 (17.4)%)	27 (27.6%)
At AEA	42 (42.9%)	29 (29.6%)	71 (72.5%)
Total	52 (53.1%)	46 (46.9%)	98 (100%)
Lateral AEA to bulla lamella vs lateral AEA to basal lamella of the middle turbinate			
	Basal Lamella of the Middle Turbinate		
Bulla Lamella	Separate from AEA	At AEA	Total
Separate from AEA	28 (28.6%)	24 (24.5%)	52 (53.1%)
At AEA	39 (39.8%)	7 (7.1%)	46 (46.9%)
Total	67 (68.4%)	31 (31.6%)	98 (100%)

ver, using this plane alone would pose difficulties in accurately identifying the lamella to which the AEA is related. The axial plane will show the angulation of the path the artery follows in the ethmoid and/or skull base, and the sagittal plane will display with accuracy, especially if one " scrolls" back and forth through the sagittal images, the relationship between the AEA and the bulla lamella and/or the basal lamella of the middle turbinate. The variability of the AEA correlates with the variability of the sinuses and particularly the ethmoid anatomy. The above-mentioned authors, as well as others, used various displays of the CT data, and cadaveric dissection information in an attempt to establish anatomic "landmarks" that would aid the endoscopic sinus surgeon with identification and subsequently avoid inadvertent traumatization to the AEA.

Several authors have described intraorbital, intracranial, and intraethmoid structures as potential landmarks on CT images defining the location of the AEA. However, most of these "potential landmarks "preclude accurate endoscopic guidance during surgery and fail to adequately identify the location of the artery [4,8,12,13,14-21]. Several authors describe the AEA to be between the second and third lamellae, that it may course in the skull base, or bellow skull base, and that the distance from skull base to the artery is greater on the right side [4, 6, 12]. Erdogmus et al. described the positional relationship between the AEA and the PEA to be 10-17 mm, with a mean distance of 13mm, and that the location of the AEA is immediately posterior to the frontal recess [13]. Simmen et al., however, in their cadaveric study, found that the AEA was approximately 11 mm from the posterior wall of the frontal recess (ranging from 6-15 mm), and concluded that the artery is found between the second and third lamellae [15]. In our study, we found the AEA to be adhearant or lose to either

Table 5. Confusion matrix for class membership: medial vs lateral AEA to the base of the skull.

Medial AEA to the base of the skull vs lateral AEA to the base of the skull			
	Medial Base of the Skull		
Lateral Base of the Skull	Separate from AEA	At AEA	Total
Separate from AEA	31 (31.6%)	15 (15.3%)	46 (46.9%)
At AEA	12 (12.2%)	40 (40.8%)	52 (53.1%)
Total	43 (43.9%)	55 (56.1%)	98 (100%)

Table 6. Contingency table for class membership medial vs lateral AEA to BL on the left and medial vs lateral AEA to BLMT on the right.

Medial vs lateral AEA to bulla lamella			
	Medial Bulla Lamella		
Lateral Base of the Skull	Separate from AEA	At AEA	Total
Separate from AEA	22 (22.5%)	30 (30.6%)	52 (53.1%)
At AEA	5 (5.1%)	41 (41.8%)	46 (46.9%)
Total	27 (27.6%)	71 (72.5%)	98 (100%)
Medial vs lateral AEA to basal lamella of the middle turbinate			
	Medial Basal Lamella of MT		
Lateral Base of the Skull	Separate from AEA	At AEA	Total
Separate from AEA	46 (46.9%)	21 (21.4%)	67 (68.4%)
At AEA	6 (6.1%)	25 (25.5%)	31 (31.6%)
Total	52 (53.1%)	46 (46.9%)	98 (100%)

the bulla lamella or the basal lamella of the middle turbinate, also that the bulla lamella in the predominant instances defined the posterior boundary of the frontal recess. Stammberger located the AEA 1–2 mm behind the junction of the posterior wall of frontal recess and within the adjacent anterior ethmoid air cell [2]. It has been reported that the AEA is missing in 5-10% of cases [13,14]. In our study, there was a single side where the AEA could not be identified (1%).

The anatomic landmarks that were identified and reported to be related to the AEA location are part of the skull base, orbital, and frontal-ethmoid anatomy, and are concealed in the initial endoscopic view, and therefore, preclude the surgeon from accurately identifying the location of the AEA, and thus, introduce the possibility of inadvertent damage.
Our aim was to establish specific anatomic landmarks definable at the initial steps of the endoscopic-guided procedure, and provide the surgeon with a step-by-step guide that would lead to the AEAOur suggested approach is outlined in our methods section and describe a step by step guide in using CT MPR as well as 3D CTSI to identify the AEA foramen and the AE sulcus locations as well as the relationship to ethmoid structures.

We highlight a number of analysis features. As shown in Figure 7 all of our measurements displayed a bimodal behavior with a sharp narrow peak centered at the lamella of interest or the skull base and a second broader peak distributed a ways away from the reference structure. The sharp peak suggests that in many people the location of the AEA is not randomly located. We conjecture that the correlation between ethmoid bone anatomy and the AEA must be driven by an embryologic development strategy. The second portion of the histogram has some recognizable structure to it, in that it is shaped like a bell curve. This suggests that, for the remaining patients, the distance measured between the reference structure and the AEA is highly variable; that the most likely separation between these two structures will be at the mode or peak of the bell curve; and that we were less likely to measure separations smaller than or larger than the mode. This second behavior suggests the driving factors during development maybe weakly coupled rather than causal or there maybe multiple strategies that leading to different morphologies.
one the less, the bimodal distribution implies that there are two distinct morphologic classes of human anatomy. Since the data is not unimodal, unimodal analysis techniques, such as those presented in Table 1, result in uncontrolled averages of population subtypes, and are, therefore, difficult to apply to individual patients. The benefit of the Gaussian mixture model approach is that patient subtypes are automatically defined. These results are, therefore, applicable to individuals, as long as the subtype can be identified by the operating surgeon. The finite mixture model results, shown in Table 2, were used to estimate the probability that an individual would fall into one of the two classes (touching and separate). Assuming the classes can be modeled by a normal distribution, i.e., the bimodal distribution can be deconstructed into two normal distributions, then the class response model, Table 3, gives us the mean or mode distance and variance of the measurements for each class. That is, the regression constant provides the most likely distance between the artery and the structure of interest for the class in question. The variance term tells us how much spread there was in our measurements - that is, how different subjects in the class of interest were from each other.
The anterior ethmoidal sulcus and the anterior ethmoidal foramen are important surgical landmarks because improper or imprecise surgery in these locations is associated with intracranial and orbital complications [4-6]. To perform safe surgery, a surgeon must have a good understanding of the local anatomy surrounding these structures and must maintain orientation at all times

while operating in these locations. We present a radiographic study of the important lamellar landmarks: the BL; the BLMT; and the surrounding structures. Our findings have a number of important implications for safe surgery. Our most important finding is that not all people are created in the same fashion, rather the anatomy can be classified into two distinct varieties: those whose anterior ethmoidal sulcus and or anterior ethmoidal foramen are associated with a lamella and those whose AEF and AES are separate from a lamella. To complicate matters, the lamella associated with the AEF can be different from the lamella associated with the AES. In addition, unlike inferiorly in the nose, where the BL and the BLMT tend to be distinct structures, they can fuse superiorly in the nose, making them less specific landmarks. This coalescence of structures is more common medially. Surgeons unaware of this behavior may be more apt to become disoriented once the inferior lamella have been resected. It is our recommendation that, if skeletonization of the AEA is necessary, the surgeon comprehensively familiarizes him/herself with the AEA and surrounding lamellar structures and the variability presented in this paper to prevent disorientation and potential injury to these structures.

Finally, there are two key anatomic findings of this study. First, populations of humans have at least two distinct architectural subtypes, in our case, subjects whose AEA, i.e., AEF and AES, are intimately associated with one or more lamellae and those whose AEA are distinct from these structures. This is important because studies that fail to account for this observation are subject to confusion. The second major finding is that, within subpopulations, human anatomic design is quite ordered. This is reflected by the fact that our measurements were easily modeled by a normal distribution. This implies that the measured separations have a most probable value, and that, as one exceeds or comes closer to the expected distance, the chance of finding the AEA decreases. The rate that this chance decreases is defined solely by the standard deviation of the distribution. This lends itself to a natural strategy for searching for the artery, i.e., the search should begin where the probability to find it is highest. We hypothesize that expert surgeons naturally learn these rules of anatomy through experience, but sometimes have difficulty implementing these rules due to the complexities introduced by the mixed nature of patient populations.

Conclusions

1. The AEA is directly related to the bulla lamella or the basal lamella.
2. Using CTMPR, if the course of the artery is carefully traced on the axial and the coronal displays, although time-consuming, and necessarily mandates the use of the MPR display, will show the relationship of the AEA to the lamellae, and this can be used to guide the FESS procedure, and preclude incursion into the artery.
3. The 3DCTSI provides an improved, more realistic, and more intuitive anatomic display of the regional anatomy, with improved correlation between the imaging display and the endoscopic view, affording improved endoscopic trailing of an, at times, convoluted course, of the anterior border of the ethmoid bulla and the bulla lamella.
4. In a large number of subjects, the BL and the AEA are either touching or nearly touching at the anterior ethmoidal foramen. Defining the above-described imaging landmarks of the AEA should be a prerequisite prior to performing FESS.
5. Along the lamina papyracea, 71.4% of the time the AEA will be associated with at least one lamella and, 7.1% of the time it will be associated with both lamellae, i.e., the AEA, the BL, and BLMT will fuse into one complex. Similarly, with our medial measurements, we found that, in 89.8% of our cases, the AEA was associated with at least one lamella and that, in 29.6% of cases, it will be associated with both lamellae.
6. The AEA is more likely to be associated with the BL than with the BLMT. More specifically, the AEA abuts the BL 72.5% medially and 46.9% laterally; while it only touches the BLMT 46.9% medially and 31.6% laterally.
7. The chance that the AEA is embedded in the BS both medially and laterally is 40.8%. In 31.6% of cases, the AEA is separate from the BS on both sides; while, in the remaining 27.5% of cases, it is attached to the BS at one end, but not the other.
8. In 35.7%, the AEA was associated with the BL at one end, but not the other. For the BLMT, this finding occurred at a slightly lower frequency of 27.5%. We found that it was more likely for an AEA that was separate from a lamella laterally to join a lamella medially than vice versa.
9. In 48.0% of subjects, the medial and lateral AEA measurement points were in the same coronal plane. In the remaining subjects, the artery ran in an oblique plane with the anterior ethmoidal sulcus, displaced, on average, 0.3 cm anterior to the anterior ethmoidal foramen.

Acknowledgement

We would like to thank Mary McAllister for editing this this manuscript. Her help is much appreciated.

Authorship contribution

SJZ initiated the project, analyzed the data, helped with study design, and wrote the manuscript. MI helped with study design, analyzed and interpreted the dataset, and assisted in the creation of the manuscript. MS helped with the conversion of the CT dataset into a 3D stereoscopic display. HS and WB helped to write the manuscript, and with study design and interpretation of the dataset. All authors read and approved the final manus-

cript.

Conflict of interest

The authors declare that this research was conducted in the absence of any commercial or financial relationships that could be construed as a potential conflict of interest.

Ethics approval and consent to participate

Not applicable.

Consent for publication

Not applicable

Availability of data and materials

Not applicable.

Funding

Not applicable.

References

1. Messerklinger W. Role of the lateral nasal wall in the pathogenesis, diagnosis and therapy of recurrent a chronic rhinosinusitis. Laryngol Rhinol Otol (Stuttg) 1987;66:293Y299 [in German]
2. Stammberger H, Posawetz W. Functional endoscopic sinus surgery. Concept, indications and results of the Messerklinger technique. Eur Arch Otorhinolaryngol 1990;247:63Y76
3. Kennedy DW, Zinreich SJ. The functional endoscopic approach to inflammatory sinus disease: current perspective and technique modifications. Am J Rhinol 1988; 2: 89–96.
4. Hosemann W, Draf C. Danger points, complications and medico-legal aspects in endoscopic sinus surgery. GMS Current Topics in Otorhinolaryngology-Head and Neck Surgery 2013;12:5-61
5. Suzuki S, Yasunaga H, Matsui H, Fushimi K, et al. Complication rates after functional endoscopic sinus surgery: analysis of 50,734 Japanese patients. Laryngoscope.2015 Aug;125(8):1785-91.
6. Lund V, Wright A, Yiotakis J, Complications and medicolegal aspects of endoscopic sinus surgery. Journal OF THE Royal Society of Medicine 1997;90:422-428
7. Zinreich SJ, Kennedy DW, Rosenbaum AE, et al. Paranasal sinuses: CT imaging requirements for endoscopic sinus surgery. Radiology 1987; 163:769-75
8. Gotwald TF, Mentzler A, Beauchamp NJ, Nedden D, Zinreich SJ. Paranasal and orbital anatomyrevisited:identification of the ethmoid arteries on coronal CT scans.Crit Rev Comput Tomogr: 2003;44:263-82
9. Sanudo JR, Vasquez R, Puerta J, Meaning and clinical interest of the anatomical variations in the 21st century; Eur J Anat. 2003; 7 suppl 1: 1-3
10. Kainz J, Stammberger H. The roof of the anterior ethmoid: a place of leastresistance in the skull base. Am J Rhinology 1989; 4:191-199
11. Lund VJ, Stammberger H, Fokkens WJ, Beale T, Bernal-Sprekelsen M, Eloy P, et al. European position paper on the anatomical terminology of the internal nose and paranasal sinuses. Rhinology Supplement. 2014(24):1-34.
12. Welch KC, Palmer JN, Intraoperative Emergencies During Endoscopic Sinus Surgery: CSF Leak and Orbital Hematoma. Otolaryngology Clin N Am 2008;41:581-96
13. Basak S, Karaman CZ, Akdilli A, Mutlu C, Obadashi o, Erpek G. Evaluation of some important anatomical variationsand dangerous areas of the paranasal sinuses by CT for safer endonasal surgery. Rhinology.1998Dec;36(4):162-7
14. Erdogmus S, Govsa F. The anatomic landmarks of ethmoidal arteries for the surgical approaches. J Craniofac Surg. 206; 17:280-5
15. Simmen D, Raghavan U, Briner HR, Manestar M, Schuknecht B, Groscurth P, Jones NS. The surgeon's view of the anterior ethmoid artery. Clin Otolaryngol. 2006 Jun;31(3):187-91.
16. Cankal F, Apaydin N, Acar HI, Elhan A, Tekdemir I, Yurdakul M, Kaya M, Esmer AF. Evaluation of the anterior and posterior ethmoidal canal by computed tomography. Clin Radiol. 2004 Nov;59(11):1034-40.
17. Han JK, Becker SS, Bomeli SR, Gross CW. Endoscopic localization of the anterior and posterior ethmoid arteries. Ann Otol Rhinol Laryngol. 2008 Dec;117(12):931-5.
18. Yang YX, Lu QK, Liao JC, Dang RS. Morphological characteristics of the anterior ethmoidal artery in ethmoid roof and endoscopic localization. Skull Base. 2009;19:311-317.
19. Zhang L, Han D, Ge W, et al. Computed tomographic and endoscopic analysis of supraorbital ethmoid cells. Otolaryngol Head Neck Surg. 2007;137:562-568.
20. Jang D W, , Vasileios A. Lachanas, White C W, Kountakis S E,; Supraorbital Ethmoid Cell: A Consistent Landmark for Endoscopic Identification of the Anterior Ethmoidal Artery; Otolaryngology–Head and Neck Surgery Otolaryngology–Head and Neck Surgery 2014, Vol. 151(6) 1073–1077
21. Moon H.J., Kim H.U., Lee J.G. et al. (2001) Surgical anatomy of the anterior ethmoid roof. Laryngoscope 111, 900–904

S. J. Zinreich
The Russel H. Morgan Department of Radiology
The Johns Hopkins Medical Institutions
Baltimore
MD, USA

E-mail: sjzinreich@jhmi.edu